



Disruption of canonical AHR-mediated induction of hepatocyte PKM2 expression compromises antioxidant defenses and increases TCDD-induced hepatotoxicity

Karina Orłowska^{a,b}, Rance Nault^{a,b,c}, Jesmin Ara^a, John J. LaPres^{a,b}, Jack Harkema^{c,d}, Elena Y. Demireva^{e,f}, Huirong Xie^{e,f}, Rachel H. Wilson^g, Christopher A. Bradfield^g, Dianne Yap^{h,2}, Aditya Joshi^{h,1}, Cornelis J. Elferink^h, Tim Zacharewski^{a,b,*}

^a Biochemistry & Molecular Biology, Michigan State University, East Lansing, MI, 48824, USA

^b Institute for Integrative Toxicology, Michigan State University, East Lansing, MI, 48824, USA

^c Department of Pharmacology and Toxicology, Michigan State University, East Lansing, MI, 48824, USA

^d Department of Pathobiology and Diagnostic Investigation, Michigan State University, East Lansing, MI, 48824, USA

^e Transgenic and Genome Editing Facility, Michigan State University, East Lansing, MI, 48824, USA

^f Institute for Quantitative Health Science & Engineering, Michigan State University, East Lansing, MI, 48824, USA

^g McArdle Laboratory for Cancer Research, University of Wisconsin-Madison, Madison, WI, 53706, USA

^h Department of Pharmacology and Toxicology, The University of Texas Medical Branch at Galveston, Galveston, TX, 77550, USA

ABSTRACT

Metabolic reprogramming by the pyruvate kinase M2 isoform is associated with cell proliferation and reactive oxygen species (ROS) defenses. 2,3,7,8-Tetrachlorodibenzo-*p*-dioxin (TCDD), an environmental contaminant that induces ROS and hepatotoxicity, dose-dependently induces pyruvate kinase muscle isoform M2 (PKM2) in the liver. To further investigate its role in combating TCDD hepatotoxicity, a Pkm^{ADRE} mouse was constructed lacking the dioxin response element mediating aryl hydrocarbon receptor (AHR) induction. TCDD failed to induce hepatic PKM2 in Pkm^{ADRE} mice and in primary hepatocytes isolated from an AHR knockout model (AHR^{V375Afl/fl}Alb-Cre^{ERT2}), demonstrating induction is AHR dependent. Both wild-type (WT) and Pkm^{ADRE} mice exhibited dose-dependent increases in liver weight after treatment with TCDD every 4 days for 28 days. Glutathione (GSH) levels increased in WT mice while oxidized glutathione (GSSG) levels increased in both models with a 24-fold decrease in the GSH/GSSG ratio in Pkm^{ADRE} mice suggesting lower antioxidant and recycling capacity. Moreover, TCDD-induced fibrosis was more severe in Pkm^{ADRE} mice while Pkm^{ADRE} hepatocytes exhibited greater cytotoxicity following co-treatment with TCDD and hydrogen peroxide. TCDD also induced PKM2 in human HeparG™ cells with AHR enrichment at a conserved DRE core within the locus. These results suggest AHR-mediated PKM2 induction is a novel antioxidant response to TCDD.

1. Introduction

2,3,7,8-Tetrachlorodibenzo-*p*-dioxin (TCDD) is the prototypical member of a class of persistent environmental contaminants that includes polychlorinated dibenzo-*p*-dioxins, dibenzofurans and biphenyls. Toxic members include congeners with lateral chlorines that induce a diverse spectrum of species-, sex-, age-, tissue- and cell-specific effects. This includes the induction of xenobiotic metabolizing enzymes and oxidative stress as well as hepatotoxicity, immunotoxicity, reproductive and developmental defects, endocrine disruption and cancer [1]. Most,

if not all, of the effects are mediated by the aryl hydrocarbon receptor (AHR), a ligand-activated basic helix-loop-helix PER-ARNT-SIM transcription factor. Upon ligand binding, the cytoplasmic AHR is activated and translocates to the nucleus where it sheds chaperone proteins and heterodimerizes with the aryl hydrocarbon nuclear translocator (ARNT) [2]. The ligand activated AHR-ARNT complex then binds specific DNA motifs known as dioxin response elements (DREs) containing the core sequence 5'-GCGTG-3' as well as at nonconsensus sites resulting in the recruitment of coactivator complexes to gene promoters and enhancers to elicit differential expression [3,4].

* Corresponding author. Michigan State University, Department of Biochemistry & Molecular Biology, Biochemistry Building, 603 Wilson Road, East Lansing, MI, 48824, USA.

E-mail address: tzachare@msu.edu (T. Zacharewski).

¹ University of Oklahoma Health Sciences, College of Pharmacy, P.O. Box 26901, Oklahoma City, OK 73126-0901.

² KBR Inc., Suite 3400, 601 Jefferson St, Houston, TX 77002.

Recent studies report that in addition to the induction of xenobiotic metabolizing enzymes, TCDD also dose-dependently causes metabolic reprogramming in the liver. Persistent activation of AHR by TCDD elicited changes in the expression of genes associated with intermediate metabolism. For example, TCDD alters the expression of pyruvate kinase (PK, EC 2.7.1.40), a rate-limiting enzyme in glycolysis which catalyzes the conversion of phosphoenolpyruvate to pyruvate. The PK family consists of four isoforms encoded by two separate genes. PKL (liver) and PKR (erythrocytes) are encoded by the *Pklr* gene while the *Pkm* gene encodes both the M1 and M2 isoforms. The *Pkm* gene spans ~32 kb and consists of 12 exons and 11 introns. The M1 and M2 isoforms are expressed following the mutual exclusion of exons 9 (M1) and 10 (M2), respectively [5]. PKM1 is a constitutively expressed, high activity PKM

isoform, whereas PKM2 exists as either a high-activity tetramer or low-activity dimer [6]. Tetrameric PKM2 possesses PKM1-like activity when stabilized with fructose-1,6-bisphosphate, whereas the PKM2 dimer has lower activity [7]. PKM2 has also been identified in mitochondria and can translocate to the nucleus where it is reported to regulate gene expression [8,9]. The multifaceted activities of PKM2 highlight its important roles in cellular metabolism and gene regulation to maintain energy homeostasis.

PKM2 expression is typically associated with the Warburg effect, a common feature of cancer cells with induced glycolytic flux characterized by increased glucose uptake and fermentation to lactate regardless of the presence of oxygen. Such metabolic reprogramming promotes growth, survival, proliferation, and long-term maintenance of cancer

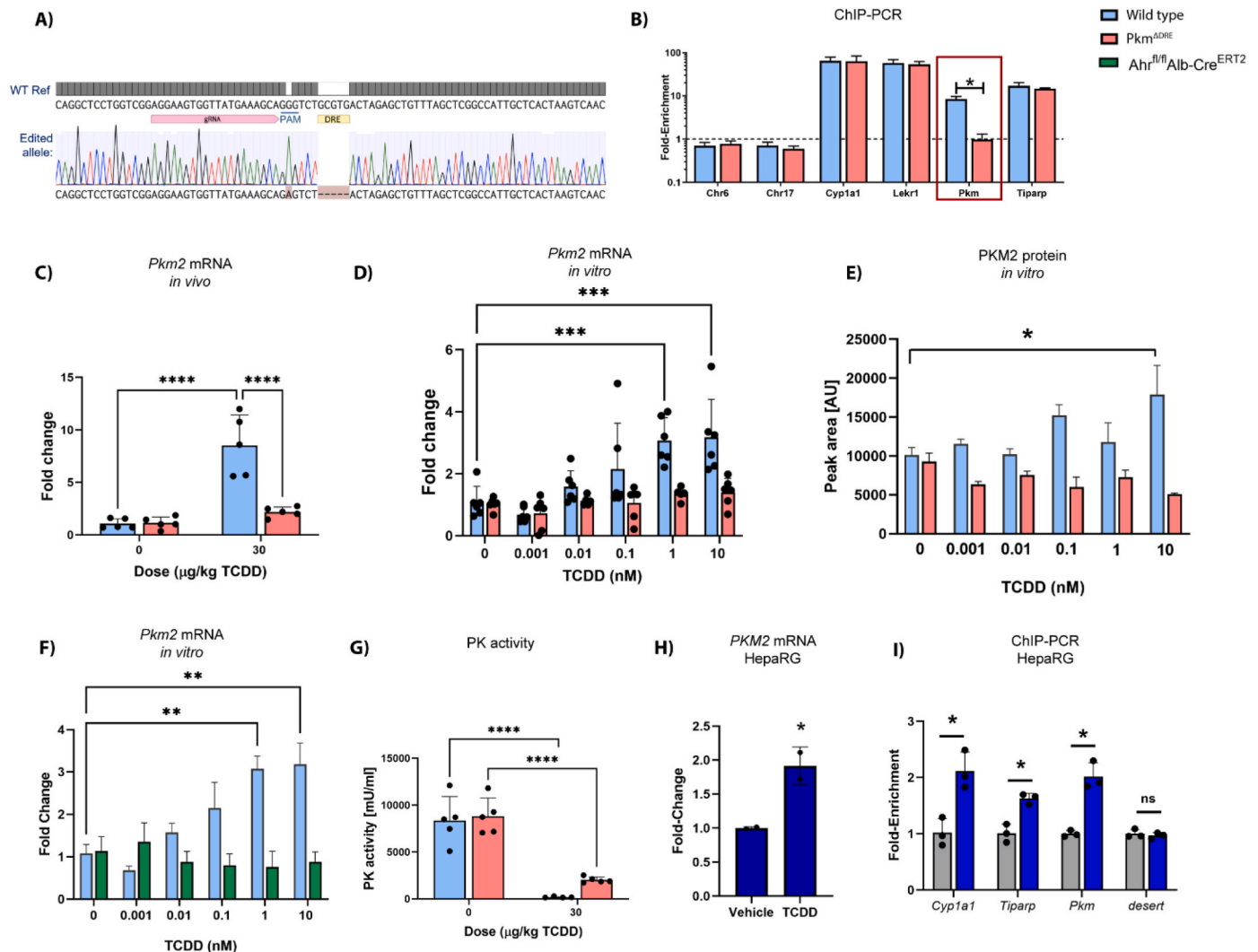


Fig. 1. *Pkm*^{ΔDRE} mice development and validation. **A)** CRISPR-Cas9 was used to specifically delete the 5bp DRE core (5' – GCGTG – 3') in the pDRE located in the *Pkm* locus (mm10:chr9:59,668,103–59,668,107). Protospacer of gRNA is annotated, PAM – underlined sequence, a single G > A mutation in the PAM was caused to prevent re-cutting of the targeted allele. Sanger sequencing of the edited allele is aligned with the reference sequence to demonstrate the DRE deletion. **B)** Hepatic AHR enrichment in mice at 2 h following oral gavage with either sesame oil vehicle (control) or 30 μg/kg TCDD measured by CHIP-PCR. **C)** The *in vivo* effect of TCDD on *Pkm2* mRNA expression assessed in livers from wild type (WT, blue) and *Pkm*^{ΔDRE} (red) mice. **D)** The *in vitro* effect of TCDD on *Pkm2* mRNA expression in isolated WT and *Pkm*^{ΔDRE} primary mouse hepatocytes (n = 5) treated for 24 h. **E)** The dose dependent *in vitro* effect of TCDD on PKM2 protein levels in isolated WT and *Pkm*^{ΔDRE} primary mouse hepatocytes (n = 5) treated for 24 h. **F)** The dose dependent effect of TCDD on *Pkm2* mRNA expression after 24 h on primary hepatocytes isolated from AHR^{V372Alf/Alf}Alb-Cre^{ERT2} mice following treatment with vehicle (control) or tamoxifen (AHR null). **G)** The effect of TCDD on pyruvate kinase (PK) activity assessed in liver extracts from wild type (WT, blue) and *Pkm*^{ΔDRE} (red) mice orally gavaged with sesame oil (vehicle) or 30 μg/kg TCDD, respectively, every 4 days for 28 days. **H)** The effect of 100 nM TCDD on PKM2 mRNA expression in differentiated human HepaRG cells (n = 2) after 24 h. **I)** AHR enrichment in human HepaRG cells after 45 min of vehicle or 100 nM TCDD treatment assessed by CHIP-PCR. A motif was identified within the enriched region (hg38: chr15:72,211,159–72,211,173) and assessed as a functional DRE. Gene expression was assessed by qRT-PCR. Protein levels were examined using an automated capillary-based immunoassay system. Bars represent mean ± standard deviation (SD). Asterisk indicates significance (* - p ≤ 0.05; ** - p ≤ 0.01; *** - p ≤ 0.001; **** - p ≤ 0.0001) determined by two-way ANOVA and Tukey's post-hoc test for panels A–G and I, and *t*-test for panel H.

cells [10]. In non-cancer cells, glycolytic flux is not induced, and therefore the increased expression of PKM2 reduces glycolytic flux causing the accumulation of upstream glycolytic intermediates that can be redirected to other pathways including the pentose phosphate pathway (PPP) and serine/glycine biosynthesis. Serine-derived one-carbon units feed into the folate cycle which also produces NADPH [11, 12]. Redirection of accumulating intermediates to the PPP and serine metabolism facilitates antioxidant responses to support glutathione (GSH) production and oxidized GSH (GSSG) recycling in response to increasing ROS levels. AHR agonists such as TCDD, 3',4,4',5-penta-chlorobiphenyl (PCB126), 2,3,7,8-tetrachlorodibenzo-furan (TCDF), and β -naphthoflavone (β -NF) are known inducers of oxidative stress that also induce *Pkm2* mRNA and protein levels [12]. In contrast, 2,2',4,4',5,5'-hexachlorobiphenyl (PCB153), a congener that does not bind nor activate AHR, fails to induce *Pkm2* expression [12]. Independent ChIP-seq, ChIP-chip and ChIP-PCR assays all show that TCDD-activated AHR binds to an intronic enhancer in the mouse *Pkm* locus at a DRE core sequence [12] suggesting *Pkm2* induction by TCDD is AHR-dependent. In the present study, we developed a genetically engineered mouse lacking the 5'-GCGTG-3' DRE core sequence within the *Pkm* locus (*Pkm*^{ADRE}) and used a high affinity AHR null model to examine the hypothesis that TCDD-induced PKM2 mediated by AHR supports antioxidant responses. The results suggest AHR-mediated PKM2 induction is an important defensive response to TCDD hepatotoxicity that is conserved between mice and humans.

2. Materials and methods

2.1. Generation of *Pkm*^{ADRE} mice

Multiple independent AHR genomic binding studies identified a single intronic peak that contains a putative DRE core sequence located between exon 3 and 4 within the *Pkm* locus suggesting direct AHR-mediated regulation [4,12]. In the present study, this intronic DRE (mm10:chr9:59,668,103–59,668,107) was deleted using CRISPR-Cas9 genome editing to create a *Pkm*^{ADRE} mutant mouse (Fig. 1A). A guide RNA (gRNA) with a sequence and PAM 5'-AGGAAGTGGTTATGAAAGCA GGG-3' targeting the intronic DRE sequence upstream of exon 4 within the *Pkm* locus was used to create a double strand break 9bp upstream of the DRE. A single-stranded oligodeoxynucleotide (ssODN) donor template (5'-; CAGGATTTGTGTTTGAA-GATTTCTGCCCTGGCAGCCTCTATCTGTTTCTACTATCGATCCCACTG-CAATTCAAACTCAAAGCTGTTGACTTAGTGAGCAATGGCCGAGCTAAA-CAGCTCTAGTAGACtCTGCTTTCATAACCACTTCTCCGACCAGGAGCCT-GCCCCGGTGCAAC-3') incorporated a 5'-GCGTG-3' motif deletion and a G > A mutation in the PAM to prevent re-cutting of the targeted allele by Cas9. Validated gRNA, Cas9 protein, and ssODN were delivered to C57BL/6 N zygotes via electroporation to generate founder animals resulting in pups with the targeted DRE deleted using established methods [13]. Following confirmation of the deletion of DRE by Sanger sequencing, animals were backcrossed for 8 generations with C57BL/6 N wild-type (WT) mice and subsequently bred to homozygosity, to generate congenic *Pkm*^{ADRE} mice. No phenotypic or behavioral abnormalities were observed in homozygous mutant mice. The homozygous mutant mice were striking similar their WT counterparts regarding somatic development, nutritional intake, and reproductive capacity. WT control mice were generated by backcrossing mutants with C57BL/6 N mice. All animal procedures were in accordance with the Michigan State University (MSU) Institutional Animal Care and Use Committee (IACUC; PROTO202100219).

2.2. Generation of *Ahr*^{fl/fl}*Alb-Cre*^{ERT2} mice

Mice homozygous for floxed *Ahr*^{V375A} (*Ahr*^{V375Afl/fl}, Jackson Laboratory strain designation B6.129(Cg)-*Ahr*^{em1Bra}/J, Strain #:035734) that express a high affinity *b* allele form of the AHR were obtained directly from Dr. Christopher Bradfield (University of Wisconsin-Madison, Madison, WI) and backcrossed to C57BL/6 N mice for 6 generations

[14]. Mice with a Cre recombinase fused to a mutant estrogen receptor ligand binding domain that requires activation by tamoxifen for activity (*Alb-Cre*^{ERT2}, strain designation B6.*Alb-Cre-ERT2*) were obtained from Dr. Cornelis Elferink (University of Texas Medical Branch, Galveston, TX) to delete floxed regions to generate null models primarily in hepatocytes [15]. To generate hepatocyte-specific *AHR*^{V375A} knockout mice (*AHR*^{V375Afl/fl}*Alb-Cre*^{ERT2}), male *AHR*^{V375Afl/fl}*Alb-Cre*^{ERT2} mice were crossed with C57BL/6-back-crossed *AHR*^{V375Afl/fl} females. Pups were genotyped and only Cre recombinase hemizygotes were used in the study. To induce *Ahr*^{V375A} ablation, *AHR*^{V375Afl/fl}*Alb-Cre*^{ERT2} mice were injected intraperitoneally with 75 μ g/kg tamoxifen for five consecutive days, followed by 5 recovery days to allow tamoxifen clearance before primary hepatocyte isolation.

2.3. Animal treatment and tissue collection

Male *Pkm*^{ADRE} and WT mice were housed in Innovive Innocages (San Diego, CA) containing ALPHA-dri bedding (Shepherd Specialty Papers, Chicago, IL) with unlimited access to Harlan Teklad Rodent Diet 8940 (Madison, WI) chow diet and water in a 23 °C environment with 30–40 % humidity and with 12/12 h light/dark cycle. Male mice (n = 8–10) were orally gavaged between zeitgeber time (ZT) 0–3 with sesame oil vehicle or 1, 3, 10 or 30 μ g/kg TCDD every 4 day for 28 days for total of 7 treatments with the first dose administered on post-natal day (PND) 30–32. On the 28th day of the study mice were euthanized via carbon dioxide. Blood was collected by cardiac puncture, iced for 30 min and centrifuged (10,000 \times g for 10 min) to separate serum. Liver and gonadal white adipose tissue (gWAT) were excised, weighed, snap frozen in liquid nitrogen, and stored at –80 °C. Liver sections were fixed in 10 % neutral buffered formalin (Sigma-Aldrich, MO), embedded with paraffin and stained with hematoxylin and eosin (H&E) for general morphometric analysis as previously described [16]. F4/80 was performed to determine inflammation, and PicroSirius Red (PSR) to verify collagen deposition based on protocols available online (<https://www.bio-rad-antibodies.com/indirect-immunostaining-of-paraffin-embedded-tissue-sections.html> and <https://ihcworld.com/2024/01/26/sirius-red-staining-protocol-for-collagen/>). F4/80 staining was performed using following antibodies Monoclonal Rat anti – Mouse F4/80 Clone: CI:A3-1 – IgG2b (MCA497G) and Goat anti Rat IgG2b antibody (STAR114P). All histological processing was performed at the Michigan State University Investigative HistoPathology Laboratory (humanpathology.msu.edu/histology). Histological severity scoring of H&E stained liver sections was performed by a certified veterinary pathologist using the following scale: 0: Minimal (<10 % of liver affected), 1: Mild (10–25 % of liver affected), 2: Moderate (25–50 % of liver affected), 3: Marked (50–75 % of liver affected), 4: Severe (75–100 % of liver affected). Quantitation of F4/80 and PSR staining intensity used QuPath and the Quantitative Histological Analysis Tool [17], respectively.

2.4. Chromatin immunoprecipitation assay (ChIP)

The truChIP Tissue Chromatin Shearing Kit (Covaris, Woburn, MA) was employed to prepare hepatic chromatin. Briefly, frozen liver samples (~120 mg) were homogenized in cold PBS using a Polytron PT2100 homogenizer (Kinematica). Protein-DNA complexes were cross-linked with 1 % formaldehyde for 10 min, followed by chromatin shearing (10 min for liver; 13 min for HepaRG cells) in a 1 mL AFA Fiber milliTUBE using the M220 Focused-Ultrasonicator (Covaris). The size distribution of double-stranded DNA fragments was evaluated using the Agilent 2100 Bioanalyzer (Santa Clara, CA) with a DNA 1200 chip, ensuring a minimum of 70 % of fragments fell within the 150–700 bp range. To attain a final concentration of 1 %, Triton X-100 (10 %) was added to the chromatin. Immunoprecipitation of cross-linked DNA was performed using anti-AHR rabbit antibodies (BML-SA210, Enzo, Farmingdale, NY and #83200, Cell Signaling for mouse and human, respectively). Purification of the ChIP DNA was carried out using a QIAquick

PCR purification kit (QIAGEN, Hilden, Germany), with subsequent elution in 40 μ L of water. Quantification of ChIP DNA and input DNA (diluted 100-fold) was performed via qRT-PCR utilizing the Bio-Rad CFX Connect Real-Time PCR Detection System (Hercules, CA). Binding to *Cyp1a1*, *Lekr*, and *Tiparp* served as positive control while regions on chromosomes 6 and 17 were negative controls. Forward and reverse primer sequences are listed in [Supplementary Table 2](#).

2.5. Clinical chemistry and serum cytokine levels

Serum cholesterol, triglyceride, and glucose levels were determined using commercially available reagents (Pointe Scientific, Canton, MI). Serum alanine aminotransferase (ALT) levels were measured using a colorimetric activity assay kit (Cayman Chemicals, Ann Arbor, MI). PK, catalase (Cat) and superoxide dismutase (Sod) activity was assessed by commercially available reagents (Abcam, Cambridge, UK; ab83432, ab83464, ab65354). Serum cytokine levels were assayed using the Luminex™ 200 system (Luminex, Austin, TX, USA) by Eve Technologies Corp. (Calgary, Alberta). Thirty-two markers were simultaneously measured using the Mouse Cytokine 32-Plex Discovery Assay® (MilliporeSigma, Burlington, Massachusetts, USA). Assay sensitivities for these markers range from 0.3 to 30.6 pg/mL for the 32-plex assay. Individual analyte sensitivity values are available from the MilliporeSigma MILLIPLX® MAP protocol.

2.6. LC-MS

Samples were analyzed as previously described with slight modifications [18]. Briefly, frozen liver samples (~20 mg) were homogenized (Polytron PT2100, Kinematica) in methanol containing 50 mM N-ethylmaleimide (NEM) and [²H₅]GSH, [¹³C₄, ¹⁵N₂]GSSG as internal standards followed by incubation at room temperature for derivatization of GSH thiols with NEM. After centrifugation, supernatant was collected, dried under nitrogen and resuspended in 0.1 % aqueous formic acid. The remaining pellet was saved for protein quantification. GSH-NEM and GSSG were separated in reversed-phase mode on an Acquity HSS T3 column (1.8 μ m, 100 \times 2.1 mm; Waters) with 0.1 % formic acid in water (solvent A) and methanol (solvent B) mobile phase gradient (0 min–100 % A, 1.5 min–100 % A, 6 min–50 % A, 6.01 min–1 % A, 7 min–1 % A; 7.01–100 % A and 8.5 min–100 % A, the flow rate 0.3 mL/min). Mass determination was performed using a Xevo G2-XS Quadrupole Time of Flight (QToF) by positive electrospray ionization. Signals were identified by retention time, accurate mass and fragmentation pattern using MassLynx Version 4.2 (Waters). Standard calibration curves for each analyte used a six-point curve of serially diluted unlabeled standards with corresponding labelled internal standards at constant concentration. Data were normalized to the protein concentration measured in the pellet remaining after metabolite isolation.

2.7. Primary hepatocytes isolation and culture

Mouse hepatocytes were isolated from AHR^{V375Al/1}Alb-Cre^{ERT2} mice treated with and without tamoxifen by perfusion and collagenase digestion [19]. In brief, the liver was perfused with calcium and magnesium-free Hanks' balanced salt solution (Sigma-Aldrich) supplemented with 0.5 mM EGTA, 5.5 mM glucose, and penicillin-streptomycin (Sigma-Aldrich) by cannulation of the inferior *vena cava*, and then with Hanks' balanced salt solution supplemented with 1.5 mM calcium chloride, 5.5 mM glucose, penicillin-streptomycin, and 0.02 % (w/v) final concentration of type IV collagenase (Sigma-Aldrich). The liver was then excised, and gently broken apart with forceps in 10 ml of William's medium E (WME; Invitrogen, Carlsbad, CA). Larger pieces and aggregated cells were removed by filtration. The resulting filtrate was centrifuged, and the hepatocyte pellet was washed three times with WME (Invitrogen). Viability was determined by trypan blue exclusion and only used when ≥ 90 %. Hepatocytes were plated at a

density of 1×10^6 cells/well in precoated type I collagen 6-well tissue culture plates containing WME with 5 % fetal bovine serum (FBS), 1 % penicillin/streptomycin, 1 % Glutamax, 0.3 mM ascorbic acid and 100 nM dexamethasone [20]. After 3 h, non-adherent cells were removed, and fresh WME containing 1 % ITS Premix Universal Culture Supplement [21], 1 % penicillin/streptomycin, 1 % Glutamax, 0.3 mM ascorbic acid and 100 nM dexamethasone were replaced. Cells incubated at 37 °C at 5 % CO₂ were then treated with TCDD for 24 h.

2.8. Computational identification of conserved DRE in humans

The evolutionarily conserved regions (ECR) browser (<https://ecrbrowser.dcode.org/>) was used to investigate the conservation of the DRE core sequence between exons 3 and 4 in the human genome [22]. The DRE core and flanking region (mm10: chr9:59,668,098–59,668,112) was used as the reference point using default settings. The genomic region was expanded to visualize conserved region annotations and identified several nearby genomic ranges. Two adjacent intronic regions overlapping with the mouse DRE core were used to extract the matching human hg19 sequence, and subsequently searched on the human hg38 genome. Examination of the extracted DNA sequence identified a DRE core within hg38:chr15:72,211,159–72,211,173.

2.9. Human HepaRG culture and differentiation

The human HepaRG™ hepatoma-derived cell line from Biopredic International (Saint-Grégoire, France) was cultured and differentiated according to previously described procedures (Aninat 2006). Briefly, HepaRG were grown in Growth Medium (GM) consisting of William's E Medium, 2 mM GlutaMAX™, 1 % penicillin/streptomycin and the addition of HepaRG™ Growth Medium Supplement (Lonza) at 37 °C, 5 % CO₂ in a humidified incubator. Media was refreshed every three days with cells passed between days 12 and 15 post seeding. HepaRG cell differentiation was initiated two weeks after passing in Differentiation Medium (DM) consisting of William's E Medium, 2 mM GlutaMAX™, 1 % penicillin/streptomycin and HepaRG™ Differentiation Medium Supplement (Lonza). GM was replaced with Combination Medium (CM), consisting of a 1:1 mixture of GM to DM, and three days later CM was replaced with DM. Medium was refreshed every three days for two weeks. After two weeks, cells attained differentiated hepatocyte-like morphology.

2.10. Cytotoxicity

Lactate dehydrogenase (LDH) was measured by the cytotoxicity detection kit (Roche Applied Science, Indianapolis, IN, USA). Primary hepatocytes were plated in 12-well culture plates and treated with DMSO vehicle or 10 nM TCDD for 24 h. Cells were treated with H₂O₂ for 48 h to induce cytotoxicity. Cells were washed with phosphate buffered saline (PBS) and lysed with 1 % triton-X-100 in PBS. LDH activity was determined in the medium and lysate by measuring absorbance at 490 nm. The LDH released into the medium was normalized to total LDH (in medium + in cell lysate).

2.11. RNA isolation and quantitative real-time polymerase chain reaction (qRT-PCR)

Primary mouse hepatocytes and human HepaRG cells (1×10^6 cells) were plated in 6-well plate for RNA isolation. Medium was removed and cells were rinsed two times with cold PBS. While on ice, 1 mL of TRIzol reagent was added to each well and plates were scraped. RNA was extracted using an additional 5:1 phenol:chloroform step (Sigma Aldrich, St. Louis, MO). RNA quantity and purity (260/280 ratio) was assessed with a NanoDrop 1000. Total RNA was converted to cDNA with SuperScript II (Invitrogen, Carlsbad, CA) using oligo dT primer. qRT-PCR was performed using iQ SYBR Green Supermix (BioRad, Hercules,

CA) on a Bio-Rad CFX Connect Real-Time PCR Detection System. Gene expression relative to vehicle control was calculated using the $2^{-\Delta\Delta CT}$ method, where each sample was normalized to the geometric mean of 3 housekeeping genes (*Actb*, *Gapdh*, and *Hprt*). SYBR green Mastermix (Life Technologies) was used to analyze relative gene expression.

2.12. Protein extraction and quantitation

Primary hepatocytes (1×10^6 cells) were plated in 6-well plate. Medium was removed and cells rinsed two times with cold PBS. Cells were scraped and collected in cold radioimmunoprecipitation buffer with protease inhibitor cocktail (Sigma-Aldrich) and incubated with constant agitation for 30 min at 4 °C, followed by centrifugation at 4 °C for 10 min at 12,000 rpm. Supernatant was collected and stored at -80 °C. Total protein was quantitated by bicinchoninic acid assay (Sigma-Aldrich). Capillary electrophoresis via the Wes system (ProteinSimple, San Jose, CA) was used to detect PKM2 (1:65; Cell Signaling, Danvers, MA), and normalized to β -actin (ACTB) (1:65; Cell Signaling). Chemiluminescence signals were exported from Compass software (ProteinSimple) and used to calculate fold-change.

3. Results

We have previously shown that TCDD induces PKM2 mRNA and protein expression concomitant with transcriptomic and metabolomic changes suggestive of increased NADPH production in response to induced cytochrome P450 activity and ROS defenses [12]. In the current study, the role of AHR-mediated *Pkm2* induction was investigated as a novel mechanism to sustain antioxidant defenses. C57BL/6 N male mice were gavaged every 4 days for 28 days with TCDD. The TCDD dose range considered the relatively brief duration of the study, while attempting to account for (i) the lifelong cumulative exposure experienced by humans to various AHR ligands, (ii) the disparity in TCDD half-life between humans (ranging from 1 to 11 years) [23] and mice (8–12 days) [24], and (iii) likely exposure to other AHR ligands. The doses and treatment regimen resulted in hepatic TCDD levels that approached steady state and induced AHR target genes including those that increase ROS levels [25].

Model development and validation – To investigate AHR-mediated induction of *Pkm2*, the intronic DRE core sequence between exons 3 and 4 (mm10: chr9: 59,668,103–59,668,107) that was present within *Ahr* genomic sequence enriched in independent ChIP-chip, ChIP-seq and ChIP-PCR assays [4,12] was deleted using CRISPR-Cas9 genome editing (*Pkm*^{ADRE}, Fig. 1A). Sequencing verified successful excision of the DRE core sequence (5'-GCGTG-3') to generate the *Pkm*^{ADRE} mouse model. Deletion of the DRE core did not result in any apparent developmental issues or alter the basal *Pkm2* levels in low (liver and lung) or high (brain and muscle) expressing tissues (Supplementary Fig. S1). Moreover, no phenotypic or behavioral abnormalities were observed in homozygous mutant mice. Homozygous *Pkm*^{ADRE} mice were striking similar to their WT counterparts in regards to somatic development, nutritional intake, and reproductive capacity.

To test the hypothesis that the intronic DRE plays a role in *Pkm2* isoform expression following AHR activation, PND 30–32 mice were treated with 30 μ g/kg TCDD. Liver samples were collected at 2 h for ChIP-PCR analysis. AHR genomic enrichment was detected at the *Pkm* DRE as well as at characterized DREs in *Cyp1a1*, *Lekr1*, and *Tiparp* (positive controls) in WT mice [4]. In contrast, no AHR binding was detected at the deleted *Pkm* DRE motif in *Pkm*^{ADRE} mice while AHR genomic enrichment at *Cyp1a1*, *Lekr1*, and *Tiparp* DREs was unchanged, confirming the importance of the core DRE sequence for AHR binding (Fig. 1 B). Negative control regions from chromosomes 6 and 17 containing no pDRE sequence did not exhibit AHR binding.

Following confirmation of no AHR binding within the *Pkm* locus in *Pkm*^{ADRE} mice, the effect of TCDD on mRNA, protein and enzyme activity was evaluated. Basal *Pkm2* expression was compare between WT

and *Pkm*^{ADRE} mice and unlike WT mice, was not induced by 30 μ g/kg TCDD in *Pkm*^{ADRE} mice treated every 4 days for 28 days (Fig. 1C). Moreover, TCDD did not induce *Pkm2* mRNA and protein levels in primary hepatocytes isolated from *Pkm*^{ADRE} mice (Fig. 1D and E). Furthermore, TCDD did not induce *Pkm2* mRNA in primary hepatocytes isolated from AHR^{V375Alf/f}Alb-Cre^{ERT2} mice (Fig. 1 F). Total PK activity was comparable in WT and *Pkm*^{ADRE} in control liver extracts and repressed by 30 μ g/kg TCDD (Fig. 1 G). A repression of PK activity was observed in both WT and *Pkm*^{ADRE} mice following TCDD treatment. Given the need for rapid regulation of enzyme activity, the decrease in PK activity in *Pkm*^{ADRE} mice may be attributed to phosphorylation or other post-translational modifications. The greater repression of total PK activity in WT liver extracts is likely due to the TCDD-induced upregulation of PKM2, which is absent in the *Pkm*^{ADRE} mice. Collectively, these results demonstrate that (i) AHR binding to the DRE within the locus is required for *Pkm2* induction by TCDD, (ii) AHR mediates induction of *Pkm2* in hepatocytes, and (iii) the *Pkm*^{ADRE} mouse model can be used to test the hypothesis that DRE-dependent induction of PKM2 is involved in sustaining antioxidant defenses in response to TCDD treatment.

PKM2 was also induced by 100 nM TCDD after 24 h in differentiated human HepaRG cells (Fig. 1H). ChIP-PCR detected AHR genomic enrichment at a pDRE (5'-AGGTTTCAGCCATTC-3'; hg38: chr15:72,211,159–72,211,173) within the human *PKM* locus as well as at characterized DREs in *CYP1A1* and *TIPARP* (positive controls) 2 h after treatment with 100 nM TCDD (Fig. 1I). The absence of AHR binding in a desert region (negative control) confirmed the specificity of these interactions (Fig. 1I). This suggests AhR-dependent regulation mechanism of *PKM2* expression may also exist in humans and play a role in antioxidant defense. However, further investigation using more relevant human liver models is required.

Gross Morphology & Histopathology – PND 30–32 male C57BL/6 mice were orally gavaged with TCDD every 4 days for 28 days to further examine the role of *Pkm2* induction in AHR-mediated hepatotoxicity. TCDD at 30 μ g/kg decreased terminal body weight by 14 % and 11 % in WT and *Pkm*^{ADRE} mice, respectively (Table 1). There was no significant change in daily food intake (Supplementary Fig. S2). Relative liver weights (RLW) were dose-dependently increased in WT and *Pkm*^{ADRE} mice by TCDD (Table 1). In WT mice, relative gonadal white adipose tissue weight (RgWAT) values ranged from 0.015 g to 0.018 g across the TCDD doses, with no clear dose-dependent trend. In contrast, RgWAT decrease at 30 μ g/kg TCDD in *Pkm*^{ADRE} mice (Table 1). TCDD also decreased serum cholesterol levels in WT mice at 30 μ g/kg TCDD while in *Pkm*^{ADRE} mice cholesterol levels were reduced at both 10 and 30 μ g/kg TCDD (Table 1). Serum glucose and triglyceride levels decreased only at 30 μ g/kg TCDD in both genotypes (Table 1).

TCDD induced dose-dependent periportal hepatopathology characterized by (i) conspicuous mixed inflammatory cell infiltrates composed mainly of monocytes with fewer polymorphonuclear leukocytes, (ii) hepatocellular hypertrophy with vacuolization (lipid droplet accumulation), (iii) interstitial fibrosis, and (iv) occasional hepatocytes undergoing degeneration and necrosis, as previously reported [26] (Fig. 2A, Table 2). Periportal inflammation was first evident at 0.3 μ g/kg TCDD in *Pkm*^{ADRE} mice, while in WT mice, it was first evident at 3 μ g/kg TCDD (Table 2). The severity of inflammation increased in a dose-dependent manner in both strains with associated minimal/mild hepatic cell degeneration and necrosis (Table 2). Minimal bile duct proliferation was observed only in *Pkm*^{ADRE} mice at 30 μ g/kg TCDD with collagen deposition along portal tracts. Quantitative analysis of collagen deposition using PSR staining revealed a 3.2- and 4.8-fold increase in WT and *Pkm*^{ADRE} mice, respectively, at 30 μ g/kg (Fig. 2B). TCDD treatment resulted in a more pronounced upregulation of fibrosis marker genes in *Pkm*^{ADRE} mice compared to WT. qRT-PCR analysis revealed significantly higher expression levels of *Acta2* and *Col1a1* in TCDD-treated *Pkm*^{ADRE} mice relative to their WT counterparts (Fig. 2C). Specifically, *Acta2* expression increased 7.6-fold in *Pkm*^{ADRE} mice versus 4.7-fold in WT mice, while *Col1a1* showed a 6.4-fold increase in *Pkm*^{ADRE} mice

Table 1
Terminal body/tissue weight and serum clinical chemistry (n = 5).

TCDD dose (µg/kg)	0		0.3		3		10		30	
	WT	Pkm ^{ΔDRE}	WT	Pkm ^{ΔDRE}	WT	Pkm ^{ΔDRE}	WT	Pkm ^{ΔDRE}	WT	Pkm ^{ΔDRE}
Terminal body weight (g)	20.20 ± 0.31	19.24 ± 1.69	20.60 ± 1.22	20.42 ± 0.92	20.80 ± 1.53	19.48 ± 1.38	18.46 ± 1.62	19.12 ± 1.09	17.45 ± 1.54 ^a	17.14 ± 1.17 ^a
RLW	0.061 ± 0.005	0.056 ± 0.002	0.067 ± 0.004 ^a	0.067 ± 0.002 ^a	0.072 ± 0.003 ^a	0.072 ± 0.003 ^a	0.071 ± 0.003 ^a	0.073 ± 0.004 ^a	0.080 ± 0.003 ^a	0.086 ± 0.007 ^a
RgWAT (g)	0.015 ± 0.004	0.018 ± 0.004	0.013 ± 0.004	0.015 ± 0.002	0.013 ± 0.004	0.015 ± 0.003	0.014 ± 0.003	0.015 ± 0.002	0.013 ± 0.004	0.013 ± 0.002 ^a
Serum cholesterol (mg/dl)	120.91 ± 6.14	136.2 ± 7.54	128.54 ± 4.2	138.5 ± 20.32	112.56 ± 5.15	119.93 ± 8.07	96.31 ± 4.73	101.86 ± 8.67 ^a	92.27 ± 7.94 ^a	107.61 ± 14.53 ^a
Serum glucose (mg/dl)	121.1 ± 6.4	124.5 ± 9.9	124.4 ± 13.4	120.7 ± 13.7	126.8 ± 10.7	118.2 ± 5.1	109.7 ± 4.3	115.3 ± 10.0	96.4 ± 3.7 ^a	91.3 ± 2.8 ^a
Serum triglycerides (mg/dl)	68.21 ± 6.38	70.47 ± 3.90	73.80 ± 2.06	69.70 ± 2.95	77.43 ± 3.44	82.63 ± 7.95	68.56 ± 3.30	76.63 ± 13.00	55.59 ± 7.42 ^a	54.40 ± 2.18 ^a

^a depicts difference when compared to corresponding vehicle control.

compared to a 3.9-fold increase in WT mice. Gene expression associated with fibrosis is consistent with the increased PSR staining, suggesting greater collagen deposition in liver sections from Pkm^{ΔDRE} mice.

Although serum ALT levels increased at 30 µg/kg TCDD in both genotypes, there was no evidence of overt toxicity (Supplementary Fig. S3). ALT levels along with histopathology and gross morphology suggest the absence of overt toxicity following oral gavage with TCDD every 4 days for 28 days. However, the loss of PKM2 induction in Pkm^{ΔDRE} mice did appear to exacerbate TCDD hepatotoxicity as suggested by the higher RLW increase and detection of inflammation at lower TCDD doses.

Oxidative Stress and Antioxidant Defenses – Oxidative damage, increased ROS production, and the differential expression of antioxidant enzymes indicate disrupted redox balance perturbation. We hypothesized that TCDD induced PKM2 gene and protein expression would support NADPH production and defenses against ROS damage, and therefore assessed the effects of TCDD on GSH and GSSG levels. TCDD dose-dependently increased GSH levels in WT mice at 10 µg/kg and 30 µg/kg. However, GSH levels only increased at 10 µg/kg TCDD in Pkm^{ΔDRE} mice (Fig. 3A). GSSG levels increased in both WT and Pkm^{ΔDRE} mice at 30 µg/kg TCDD, but GSSG levels were 2-fold greater in Pkm^{ΔDRE} mice suggesting limited GSSG recycling in the absence of PKM2 induction (Fig. 3B). The different effects of TCDD on GSH and GSSG levels were also reflected in the GSH:GSSG ratio. Although the ratio decreased in both genotypes, the compromised ability to recycle GSSG to GSH was more pronounced in Pkm^{ΔDRE} mice (Fig. 3C). The GSH:GSSG ratio in WT mice was 2070 compared to 450 for Pkm^{ΔDRE} mice at 30 µg/kg TCDD. To further explore the role of AHR-dependent *Pkm2* induction in antioxidant defenses, WT and Pkm^{ΔDRE} primary hepatocytes were co-treated with TCDD and hydrogen peroxide. Pkm^{ΔDRE} primary hepatocytes co-treated with TCDD and H₂O₂ exhibited greater cytotoxicity (LC₅₀ 290 µM) compared to treated WT (LC₅₀ 620 µM) providing further evidence of a protective role for AHR-mediated PKM2 induction (Fig. 3D).

In addition to inducing PKM2, TCDD also regulated the expression of other genes associated with ROS defense. However, the expression of antioxidant gene was consistently muted in Pkm^{ΔDRE} mice compared to WT (Supplementary Fig. S4). For example, glutathione peroxidase 2 and 4 (*Gpx*) which protect against hydrogen peroxide and lipid peroxides, were induced by TCDD in both models, but *Gpx2* and *Gpx4* induction was ~2 times lower in Pkm^{ΔDRE} mice compared to WT. Superoxide dismutase (SOD), an enzyme involved in superoxide radical neutralization, showed a similar trend, with more modest *Sod1*, *Sod2*, and *Sod3* induction in Pkm^{ΔDRE} mice compared to WT mice. Changes in the expression of catalase (*Cat*), the enzyme responsible for hydrogen peroxide degradation, did not reach statistical significance.

CAT and SOD activities were also evaluated in liver extracts of WT and Pkm^{ΔDRE} mice. The levels of basal CAT and SOD activity in WT and Pkm^{ΔDRE} liver extracts were comparable. TCDD increased CAT activity

in WT but had a negligible effect in Pkm^{ΔDRE} liver extracts (Supplementary Fig. S5). In contrast to its mRNA induction, SOD activity decreased in both genotypes possibly due to post-translational modification, with Pkm^{ΔDRE} mice exhibiting a more pronounced decline. Weaker CAT and SOD activity responses in Pkm^{ΔDRE} mice implies a compromised ability to mount an effective antioxidant defense against persistent TCDD-induced oxidative stress consistent with increased levels of inflammation and fibrosis compared to WT mice.

Serum Cytokines – Accumulating cell damage due to ROS can activate signaling pathways that promote the production and release of pro-inflammatory cytokines, chemokines, and adhesion molecules. TCDD dose-dependently induced serum granulocyte colony-stimulating factor (G-CSF), eotaxin, interleukin 1 alpha (IL-1α) and lipopolysaccharide-induced CXC chemokine (LIX) levels in WT and Pkm^{ΔDRE} mice, which are generally considered pro-inflammatory (Fig. 4). Eotaxin, IL-1α and LIX induction was greater in Pkm^{ΔDRE} while G-CSF levels were higher in WT serum samples. G-CSF is not typically classified as pro-inflammatory or anti-inflammatory with its effects dependent on context. G-CSF plays a crucial role in regulating the production and maturation of granulocytes, particularly neutrophils which dominate the early stages of inflammation. G-CSF levels increased in both genotypes at 30 µg/kg TCDD, however, the increase was greater in WT. Serum eotaxin levels were significantly higher in Pkm^{ΔDRE} mice at 10 and 30 µg/kg TCDD compared to WT mice. The levels of IL-1α were also higher in Pkm^{ΔDRE} mice suggesting mice lacking PKM2 expression experienced greater inflammation. LIX is a cytokine primarily involved in the early stages of acute inflammation that amplifies the inflammatory response by promoting neutrophil activation. It stimulates the production of ROS and other effector molecules by neutrophils. Like IL-1α, LIX induction by TCDD was higher in Pkm^{ΔDRE} mice than in WT. Collectively, these results suggest that Pkm^{ΔDRE} mice experience more acute inflammation, consistent with the evidence of more severe fibrosis.

4. Discussion

In this study, a 5-bp DRE core sequence (5'-GCGTG-3') located between exons 3 and 4 in the mouse *Pkm* locus was deleted in both alleles using CRISPR to investigate AHR-mediated regulation of *Pkm2* expression and its potential consequences on TCDD-induced hepatotoxicity. Despite the effects of TCDD on steatosis being comparable between WT and Pkm^{ΔDRE} mice, other responses were attenuated, including antioxidant defenses in response to the induction of oxidative stress. More specifically, GSH levels were greater in WT mice whereas GSSG levels were increased in both models. Pkm^{ΔDRE} mice had a substantially lower GSH:GSSG ratio due to weaker induction of GSH levels and greater accumulation of GSSG levels suggesting reduced antioxidant capacity and higher levels of ROS due to a compromised antioxidant gene

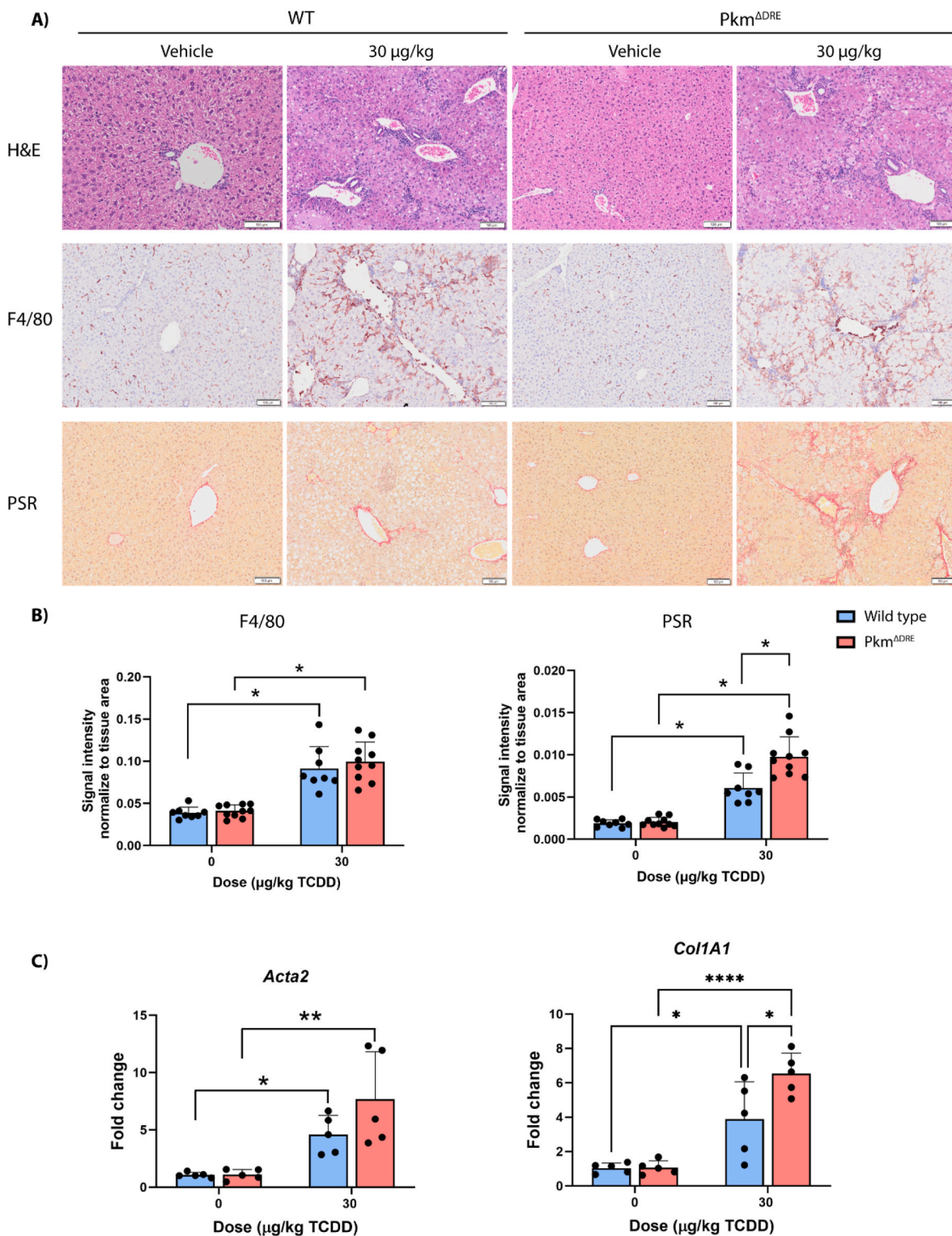


Fig. 2. Histological evaluation of liver sections from wild type (WT) and Pkm^{ADRE} mice gavaged with sesame oil vehicle or 30 µg/kg TCDD every 4 days for 28 days. (A) Representative micrographs of hematoxylin and eosin staining (H&E) to assess hepatic lesions, F4/80 to determine macrophage infiltration, and PicroSirius Red (PSR) to detect collagen deposition. Scale bar represents 100 µm. (B) Quantitation of F4/80 and PSR staining used QuPath and the Quantitative Histological Analysis Tool (n = 8–10) (Nault et al., 2015), respectively. (C) Effect of TCDD on the expression of fibrosis-related genes in male WT and Pkm^{ADRE} mice (n = 5) orally gavaged every 4 days for 28 days with TCDD. Gene expression was evaluated by qRT-PCR. Bars represent mean ± SD. Asterisk indicates significance (* - p ≤ 0.05; ** - p ≤ 0.01; **** - p ≤ 0.0001) determined by two-way ANOVA and Tukey's post-hoc test.

Table 2
Histopathological scores of H&E stained liver assessments (n = 5).

TCDD dose ($\mu\text{g}/\text{kg}$)	0		0.3		3		10		30	
	WT	$Pkm^{\Delta DRE}$								
Inflammation	0.0 \pm 0.0	0.0 \pm 0.0	0.0 \pm 0.0	0.3 \pm 0.5	0.9 \pm 0.3	0.6 \pm 0.5	2.0 \pm 0.5	1.7 \pm 0.8	2.6 \pm 0.5	2.6 \pm 0.5
Apoptosis, Necrosis	0.0 \pm 0.0	0.0 \pm 0.0	0.0 \pm 0.0	0.3 \pm 0.5	0.9 \pm 0.3	0.6 \pm 0.5	1.9 \pm 0.3	1.6 \pm 0.8	1.4 \pm 0.5	1.5 \pm 0.5
Vacuolation	0.0 \pm 0.0	0.0 \pm 0.0	0.0 \pm 0.0	0.0 \pm 0.0	0.3 \pm 0.5	0.0 \pm 0.0	3.6 \pm 0.5	2.1 \pm 1.4	3.6 \pm 0.7	4.0 \pm 0.0
Biliary Hyperplasia	0.0 \pm 0.0	0.0 \pm 0.0	0.0 \pm 0.0	1.0 \pm 0.9						
Hepatocellular hypertrophy	0.0 \pm 0.0	0.0 \pm 0.0	0.0 \pm 0.0	0.0 \pm 0.0	0.0 \pm 0.0	0.0 \pm 0.0	1.6 \pm 0.5	0.3 \pm 0.7	2.9 \pm 0.3	3.0 \pm 0.0

Histopathological grade: 0: minimal (<10 % of liver affected), 1: mild (10–25 % of liver affected), 2: moderate (25–50 % of liver affected), 3: marked (50–75 % of liver affected), 4: severe (75–100 % of liver affected).

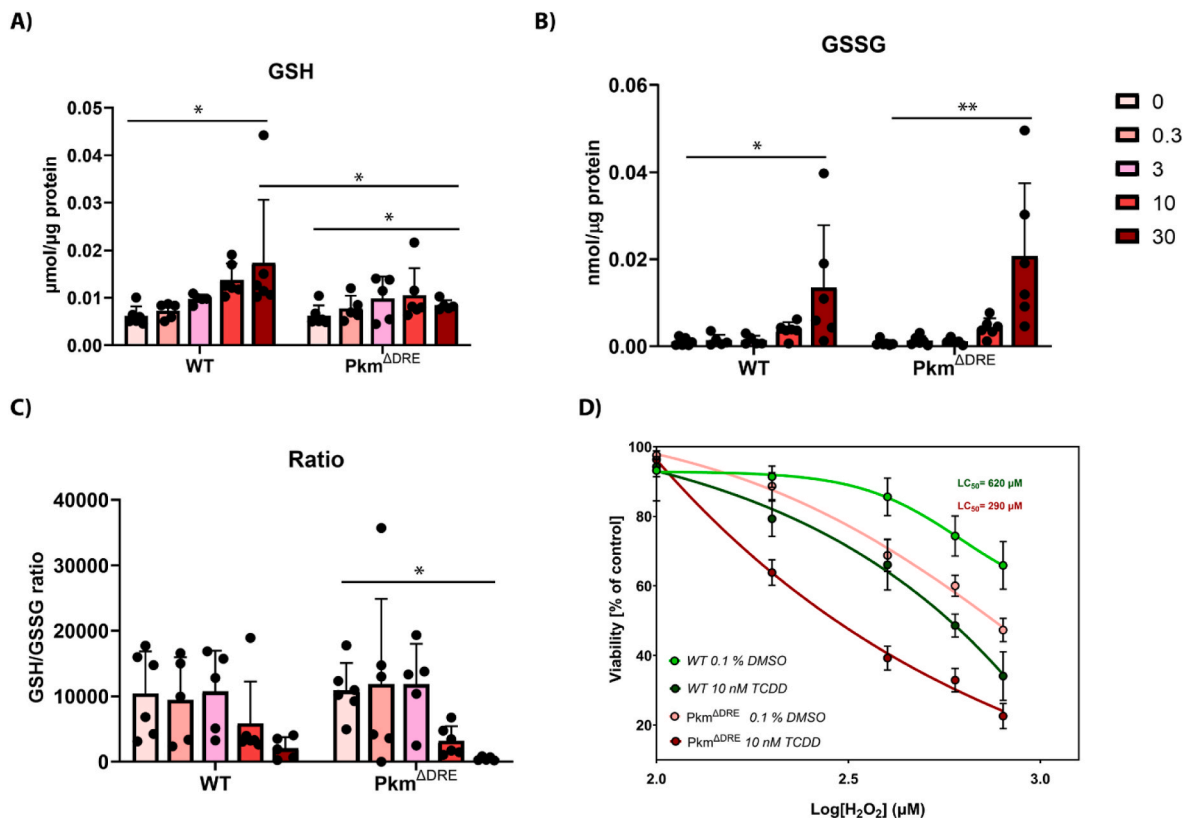


Fig. 3. Protective effect of AHR-induced PKM2. (A) Reduced (GSH) and (B) oxidized (GSSG) glutathione levels in wild type (WT) and $Pkm^{\Delta DRE}$ mice (n = 6) following oral gavage with sesame oil vehicle (control) or 0.3–30 $\mu\text{g}/\text{kg}$ TCDD. (C) GSH:GSSG ratio. Bars represent mean \pm SEM. (D) Viability of WT and $Pkm^{\Delta DRE}$ primary hepatocytes after treatment with DMSO or 10 nM TCDD for 24 h followed by cotreatment with H_2O_2 for 48 h. Bars represent mean \pm SD. Asterisk denotes significance (* p < 0.05, ** p < 0.01) determined by two-way ANOVA and Tukey's post-hoc test.

expression response. Increased collagen deposition assessed by PSR staining also indicated more severe fibrosis in $Pkm^{\Delta DRE}$ mice. Furthermore, primary hepatocytes isolated from $Pkm^{\Delta DRE}$ mice were more sensitive to H_2O_2 cytotoxicity when co-treated with TCDD. Collectively, these results suggest that the loss of PKM2 induction which exacerbated TCDD-elicited hepatotoxicity is due to reduced antioxidant defense capacity.

Whole body *Pkm* exon 10 deletion in adult male mice is reported to cause compensatory PKM1 expression, a 2-fold increase in relative liver weight and more severe steatosis in mice fed a high fat diet [27]. Furthermore, PKM2 null mice developed late-onset spontaneous hepatocellular carcinomas (HCC) with high penetrance and exacerbated hepatic inflammation in older mice (>85 weeks of age) [27]. In the current study, $Pkm^{\Delta DRE}$ mice and primary hepatocyte AHR null models were used to specifically examine *Pkm2* regulation and the effects on antioxidant responses following TCDD treatment. The targeted 5'-GCCGTC-3' sequence between *Pkm* exon 3 and 4 was identified in independent ChIP-chip, ChIP-seq and ChIP-PCR assays and deemed a

putative DRE (pDRE) when compared to characterized DREs using a position weight matrix (PWM) [4,12]. Notably, unlike the whole body exon 10 deletion model [27], there was no compensatory *Pkm1* induction in $Pkm^{\Delta DRE}$ mice (Sup. Fig. S1). Although the underlying mechanism involving exon switching in *Pkm* expression was not examined, our results show deletion of this response element did not affect basal isoform expression in the liver as well as other tissues. Likewise, ChIP-PCR detected AHR genomic enrichment at a conserved region containing a DRE core within the human *PKM* locus in differentiated human Hep-ARGTM cells 2 h after treatment with TCDD, and induction of *PKM2* mRNA at 24 h. AHR genomic binding at the pDRE and the induction of *PKM2* mRNA by TCDD suggests similar AHR-mediated PKM2 regulation may exist in humans and mice.

Metabolic dysregulation is associated with the development and progression of fatty liver disease (FLD). PKM2, a key glycolytic enzyme, has gained notoriety due to its unique roles, particularly in coordinating glycolysis during the progression of steatosis to steatohepatitis with fibrosis, a risk factor for more complex metabolic diseases including

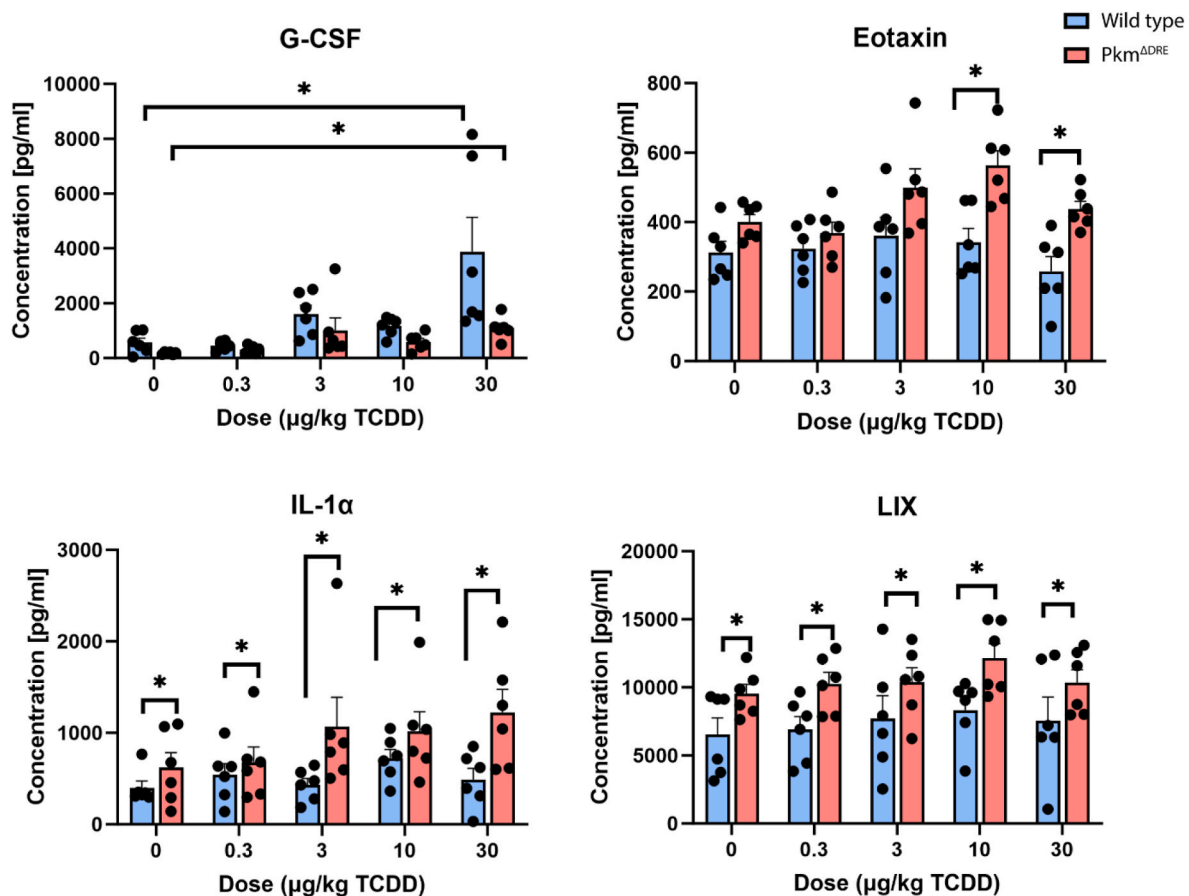


Fig. 4. Induction of cytokine levels in serum from wild type (WT) and *Pkm*^{ADRE} mice following oral gavage with TCDD (n = 6). Bars represent mean ± SD. Asterisk indicates significance (* - p ≤ 0.05) determined by two-way ANOVA and Tukey's post-hoc test.

metabolic dysfunction-associated fatty liver disease (MAFLD), end-stage liver disease and HCC [28,29]. Reports also implicate PKM2 in AHR-mediated toxicities [12,30,31]. Our previous study shows that known AHR ligands including TCDD, PCB126, TCDF, and β-NF induce *Pkm2* mRNA and protein levels. In contrast, PCB153, a non-AHR ligand, did not induce *Pkm2* in mouse [12,31] suggesting *Pkm2* induction is AHR-dependent. *Pkm2* induction was also independent of NRF2, as TCDD induction was maintained in *Nrf2* null primary mouse hepatocytes [32]. Furthermore, independent ChIP studies at 2h identified Ahr genomic enrichment in an open chromatin region between exons 3 and 4 of the *Pkm* gene further supporting AHR-mediated regulation in the mouse liver [12]. In contrast, no AHR genomic binding was detected in the same region in the *Pkm*^{ADRE} mice while genomic binding was retained within regulatory sequences containing characterized DREs in the promoters of *Cyp1a1*, *Lekr1*, and *Tiparp*. In addition, deletion of the 5'-GCGTG-3' sequence between exon 3 and 4 in the *Pkm* locus abolished the dose-dependent induction of PKM2 mRNA and protein expression in the mouse liver following treatment with TCDD. Furthermore, TCDD did not induce *Pkm2* in AHR ablated primary hepatocytes isolated from tamoxifen treated Ahr^{V375Al/Al} Alb-Cre^{ERT2} mice. These results provide compelling evidence that AHR binding to this pDRE is required for PKM2 induction by TCDD in hepatocytes.

PKM2 has the potential to form a dimer with lower enzymatic activity compared to the PKM2 tetramer as well as other pyruvate kinase isoforms. Under conditions of oxidative stress, as would be expected following TCDD treatment, PKM2 can be oxidized at Cys358 to further reduce its enzymatic activity [33]. Formation of the less active PKM2 dimer reduces glycolytic flux causing the accumulation of upstream intermediates [34]. The integration of complementary bulk RNAseq and metabolomic data from WT mice treated with TCDD suggests

accumulating glucose-6-phosphate (G6P) and 3-phosphoglycerate (3 PG) are redirected to the pentose phosphate pathway and serine/folate biosynthesis, respectively [12]. This would increase NADPH production to reduce cell injury from increasing ROS levels by supporting GSH biosynthesis and GSSG recycling [35–37]. The dose-dependent induction of GSH biosynthesis and GSSG recycling genes including *Gclc*, *Gss*, *Gpx2*, *Gpx3* and *Gsr* by TCDD as well as the increased levels of ophthalmic acid, a GSH analog with no thiol group, provides further evidence of metabolic reprogramming to maintain redox balance [25]. Together, these results show that PKM2 induction is an important enzyme in combating TCDD induced ROS levels. First, the loss of PKM2 induction compromised GSSG recycling, as indicated by the decrease in the GSH:GSSG ratio in *Pkm*^{ADRE} mice. Moreover, *Pkm*^{ADRE} mice had elevated serum levels of proinflammatory cytokines consistent with the more severe inflammation and fibrosis. In addition, primary hepatocytes isolated from *Pkm*^{ADRE} mice treated with H₂O₂ exhibited greater cytotoxicity compared to WT controls when co-treated with TCDD. Finally, CAT and SOD enzymatic activity suggests distinct oxidative stress responses between WT and *Pkm*^{ADRE} mice. The inability of *Pkm*^{ADRE} mice to increase CAT activity, combined with a larger decline in SOD activity, suggests a compromised antioxidant defense response to TCDD-induced oxidative stress. Catalase metabolizes hydrogen peroxide into water and oxygen, thus protecting the cell from oxidative damage due to accumulating H₂O₂. Furthermore, increased oxidative stress can post-translationally modify SOD leading to the inactivation or degradation creating a feedback loop where ROS further inhibits SOD activity, leading to more oxidative stress [38,39]. Overall, these results further support the hypothesis that AHR-mediated induction of PKM2 supports ROS defense responses.

The hepatic induction of genes associated with ROS defense,

specifically *Cat*, *Gpx2* and 4, and *Sod1*, 2 and 3, were also consistently lower in TCDD-treated Pkm^{ADRE} mice. In addition to metabolic reprogramming to support cell proliferation and antioxidant responses, PKM2 can also translocate to the nucleus in various cell types, where it can regulate the cell cycle, proliferation, apoptosis, and promote the onset and development of HCC [9]. Therefore, the lack of comparable TCDD effects on *Cat*, *Gpx2* and 4, and *Sod1*, 2 and 3 expression in Pkm^{ADRE} mice, compared to WT mice, may be due to the absence of nuclear PKM2 activity.

snRNAseq analysis has shown that AHR is expressed in all liver cell types including liver endothelial cells and infiltrating immune cells [40]. Consequently, the deletion of the 5'-GCGTG-3' core sequence between exon 3 and 4 in the *Pkm* locus may also affect the metabolic reprogramming and nuclear responses induced by TCDD in other cell types in Pkm^{ADRE} mice. For example, PKM2 is an important mediator of inflammation [27]. PKM2 expression can elicit metabolic reprogramming to activate immune cells and promote cytokine secretion [34]. Based on the cytokine profile, it is unclear if the *Pkm* pDRE deletion dramatically affected immune cell responses to TCDD as other mechanisms can also regulate PKM2 expression that are independent of AHR.

The integration of ChIPseq, RNAseq and metabolomics data with complementary histopathology has further elucidated mechanisms associated with the hepatic effects of TCDD beyond activation of the AHR. In addition to the induction of cytochrome P450s, increased oxidative stress and differential gene expression, recent studies have examined the dose-dependent disruption of specific metabolic pathways that result in the accumulation of reactive metabolic intermediates and contribute to the hepatotoxicity of TCDD. In response, cells mount counter measures to minimize injury, including the induction of enzymes to detoxify ROS, as well as PKM2 to support GSH biosynthesis and GSSG recycling. Consequently, the induction of PKM2 represents an important defensive counter measure, especially in response to the persistent activation of AHR by TCDD. Although these studies were predominately conducted in mouse models, we also demonstrated AHR genomic binding in the *Pkm* locus and *Pkm2* mRNA induction following treatment with TCDD in differentiated HepaRG™ cells, suggesting that the murine findings can be extrapolated to a human context.

CRediT authorship contribution statement

Karina Orłowska: Data curation, Methodology, Visualization, Writing – original draft, Writing – review & editing. **Rance Nault:** Conceptualization, Investigation, Supervision, Writing – review & editing. **Jesmin Ara:** Investigation, Writing – review & editing. **John J. LaPres:** Methodology, Supervision, Writing – review & editing. **Jack Harkema:** Investigation, Writing – review & editing. **Elena Y. Demireva:** Investigation, Methodology, Writing – review & editing. **Huirong Xie:** Investigation, Methodology, Writing – review & editing. **Rachel H. Wilson:** Investigation, Methodology, Writing – review & editing. **Christopher A. Bradfield:** Investigation, Methodology, Writing – review & editing. **Dianne Yap:** Investigation, Writing – review & editing. **Aditya Joshi:** Investigation, Writing – review & editing. **Cornelis J. Elferink:** Investigation, Writing – review & editing. **Tim Zacharewski:** Conceptualization, Funding acquisition, Project administration, Supervision, Writing – original draft, Writing – review & editing.

Funding

This project was supported by the National Institute of Environmental Health Sciences R01ES029541 to JH and TZ and R01ES033682 to CJE. TZ and JLL are partially supported by AgBioResearch at Michigan State University.

Declaration of competing interest

The authors declare that they have no known competing financial interests or personal relationships that could have appeared to influence the work reported in this paper.

Acknowledgements

We express our sincere gratitude to the members of the Transgenic and Genome Editing Facility at Michigan State University for their collaborative support and instrumental role in the creation of the Pkm^{ADRE} animal model for our studies.

Appendix A. Supplementary data

Supplementary data to this article can be found online at <https://doi.org/10.1016/j.redox.2024.103405>.

References

- [1] S. Safe, Polychlorinated-biphenyls (pcbs), dibenzo-para-dioxins (pcdds), dibenzofurans (pcdfs), and related-compounds - environmental and mechanistic considerations which support the development of toxic equivalency factors (tefs), *Crit. Rev. Toxicol.* 21 (1990) 51–88.
- [2] M.S. Denison, S.C. Faber, And now for something completely different: diversity in ligand-dependent activation of ah receptor responses, *Curr Opin Toxicol* 2 (2017) 124–131.
- [3] S.R. Wilson, A.D. Joshi, C.J. Elferink, The tumor suppressor kruppel-like factor 6 is a novel aryl hydrocarbon receptor DNA binding partner, *J Pharmacol Exp Ther* 345 (2013) 419–429.
- [4] E. Dere, R. Lo, T. Celiuș, J. Matthews, T.R. Zacharewski, Integration of genome-wide computation DRE search, AhR ChIP-chip and gene expression analyses of TCDD-elicited responses in the mouse liver, *BMC Genom.* 12 (2011) 365.
- [5] T.L. Dayton, T. Jacks, M.G. Vander Heiden, PKM2, cancer metabolism, and the road ahead, *EMBO Rep.* 17 (2016) 1721–1730.
- [6] M.A. Iqbal, V. Gupta, P. Gopinath, S. Mazurek, R.N.K. Bamezai, Pyruvate kinase M2 and cancer: an updated assessment, *FEBS Lett.* 588 (2014) 2685–2692.
- [7] W.J. Israelsen, T.L. Dayton, S.M. Davidson, B.P. Fiske, A.M. Hosios, G. Bellinger, J. Li, Y.M. Yu, M. Sasaki, J.W. Horner, et al., PKM2 isoform-specific deletion reveals a differential requirement for pyruvate kinase in tumor cells, *Cell* 155 (2013) 397–409.
- [8] X. Zhou, F. Mikaeloff, S. Curbo, Q. Zhao, R. Kuiper, A. Vegvari, U. Neogi, A. Karlsson, Coordinated pyruvate kinase activity is crucial for metabolic adaptation and cell survival during mitochondrial dysfunction, *Hum. Mol. Genet.* 30 (2021) 2012–2026.
- [9] Y.B. Lee, J.K. Min, J.G. Kim, K.C. Cap, R. Islam, A. Hossain, O. Dogsom, A. Hamza, S. Mahmud, D.R. Choi, et al., Multiple functions of pyruvate kinase M2 in various cell types, *J. Cell. Physiol.* 237 (2022) 128–148.
- [10] M.G.V. Heiden, L.C. Cantley, C.B. Thompson, Understanding the Warburg effect: the metabolic requirements of cell proliferation, *Science* 324 (2009) 1029–1033.
- [11] F.F. Diehl, C.A. Lewis, B.P. Fiske, M.G. Vander Heiden, Cellular redox state constrains serine synthesis and nucleotide production to impact cell proliferation, *Nat. Metab.* 1 (2019) 861–867.
- [12] R. Nault, K.A. Fader, M.P. Kirby, S. Ahmed, J. Matthews, A.D. Jones, S.Y. Lunt, T. R. Zacharewski, Pyruvate kinase isoform switching and hepatic metabolic reprogramming by the environmental contaminant 2,3,7,8-Tetrachlorodibenzo-p-Dioxin, *Toxicol. Sci.* 149 (2016) 358–371.
- [13] W. Qin, S.L. Dion, P.M. Kutny, Y. Zhang, A.W. Cheng, N.L. Jillette, A. Malhotra, A. M. Geurts, Y.G. Chen, H. Wang, Efficient CRISPR/Cas9-Mediated genome editing in mice by zygote electroporation of nuclease, *Genetics* 200 (2015) 423–430.
- [14] R.H. Wilson, P.R. Carney, E. Glover, J.C. Parrott, B.L. Rojas, S.M. Moran, J.S. Yee, M. Nukaya, N.A. Goetz, C.D. Rubinstein, et al., Generation of an allelic series at the AhR locus using an edited recombinant approach, *Toxicol. Sci.* 180 (2021) 239–251.
- [15] N.G. Girer, D. Carter, N. Bhattarai, M. Mustafa, L. Denner, C. Porter, C.J. Elferink, Inducible loss of the aryl hydrocarbon receptor activates perigonadal white fat respiration and Brown fat thermogenesis via fibroblast growth factor 21, *Int. J. Mol. Sci.* 20 (2019).
- [16] F.L. Carson, C. Hladik Cappellano, *Histotechnology: A Self Instructional Text*, 2009.
- [17] R. Nault, D. Colbry, C. Brandenberger, J.R. Harkema, T.R. Zacharewski, Development of a computational high-throughput tool for the quantitative examination of dose-dependent histological features, *Toxicol. Pathol.* 43 (2015) 366–375.

- [18] A. Gil, A. van der Pol, P. van der Meer, R. Bischoff, LC-MS analysis of key components of the glutathione cycle in tissues and body fluids from mice with myocardial infarction, *J Pharmaceut Biomed* 160 (2018) 289–296.
- [19] B.P. Sullivan, A.K. Kopec, N. Joshi, H. Cline, J.A. Brown, S.C. Bishop, K.M. Kassel, C. Rockwell, N. Mackman, J.P. Luyendyk, Hepatocyte tissue factor activates the coagulation cascade in mice, *Blood* 121 (2013) 1868–1874.
- [20] K.M.O. Goyak, E.M. Laurenzana, C.J. Omiecinski, Hepatocyte differentiation, *Hepatocytes: Methods and Protocols* 640 (2010) 115–138.
- [21] T. Mizuguchi, T. Hui, K. Palm, N. Sugiyama, T. Mitaka, A.A. Demetriou, J. Rozga, Enhanced proliferation and differentiation of rat hepatocytes cultured with bone marrow stromal cells, *J. Cell. Physiol.* 189 (2001) 106–119.
- [22] I. Ovcharenko, M.A. Nobrega, G.G. Loots, L. Stubbs, ECR Browser: a tool for visualizing and accessing data from comparisons of multiple vertebrate genomes, *Nucleic Acids Res.* 32 (2004) W280–W286.
- [23] W.H. Wolfe, J.E. Michalek, J.C. Miner, J.L. Pirkle, S.P. Caudill, D.G. Patterson Jr., L.L. Needham, Determinants of TCDD half-life in veterans of operation ranch hand, *J. Toxicol. Environ. Health* 41 (1994) 481–488.
- [24] T.A. Gasiewicz, L.E. Geiger, G. Rucci, R.A. Neal, Distribution, excretion, and metabolism of 2,3,7,8-tetrachlorodibenzo-p-dioxin in C57BL/6J, DBA/2J, and B6D2F1/J mice, *Drug Metab. Dispos.* 11 (1983) 397–403.
- [25] K. Orlowska, R.R. Fling, R. Nault, A.L. Schillmiller, T.R. Zacharewski, Cystine/glutamate xc⁽⁻⁾ antiporter induction compensates for transsulfuration pathway repression by 2,3,7,8-Tetrachlorodibenzo-p-dioxin (TCDD) to ensure cysteine for hepatic glutathione biosynthesis, *Chem. Res. Toxicol.* 36 (2023) 900–915.
- [26] K.A. Fader, R. Nault, M.P. Kirby, G. Markous, J. Matthews, T.R. Zacharewski, Convergence of hepcidin deficiency, systemic iron overloading, heme accumulation, and REV-ERB α /beta activation in aryl hydrocarbon receptor-elicited hepatotoxicity, *Toxicol. Appl. Pharmacol.* 321 (2017) 1–17.
- [27] T.L. Dayton, V. Gocheva, K.M. Miller, W.J. Israelsen, A. Bhutkar, C.B. Clish, S. M. Davidson, A. Luengo, R.T. Bronson, T. Jacks, et al., Germline loss of PKM2 promotes metabolic distress and hepatocellular carcinoma, *Gene Dev.* 30 (2016) 1020–1033.
- [28] D.D. Zheng, Y.C. Jiang, C. Qu, H. Yuan, K.S. Hu, L. He, P. Chen, J.Y. Li, M.X. Tu, L. H. Lin, et al., Pyruvate kinase M2 tetramerization protects against hepatic stellate cell activation and liver fibrosis, *Am. J. Pathol.* 190 (2020) 2267–2281.
- [29] M.E. Rinella, J.V. Lazarus, V. Ratziu, S.M. Francque, A.J. Sanyal, F. Kanwal, D. Romero, M.F. Abdelmalek, Q.M. Anstee, J.P. Arab, et al., A multisociety Delphi consensus statement on new fatty liver disease nomenclature, *J. Hepatol.* 79 (2023) 1542–1556.
- [30] W.L. Liang, Y.T. Zhang, L. Song, Z.Y. Li, 2,3,4,4', 5-Pentachlorobiphenyl induces hepatocellular carcinoma cell proliferation through pyruvate kinase M2-dependent glycolysis, *Toxicol. Lett.* 313 (2019) 108–119.
- [31] S. Matsuda, J. Adachi, M. Ihara, N. Tanuma, H. Shima, A. Kakizuka, M. Ikura, T. Ikura, T. Matsuda, Nuclear pyruvate kinase M2 complex serves as a transcriptional coactivator of arylhydrocarbon receptor, *Nucleic Acids Res.* 44 (2016) 636–647.
- [32] R. Nault, C.M. Doskey, K.A. Fader, C.E. Rockwell, T. Zacharewski, Comparison of hepatic NRF2 and aryl hydrocarbon receptor binding in 2,3,7,8-Tetrachlorodibenzo-p-dioxin-Treated mice demonstrates NRF2-independent PKM2 induction, *Mol. Pharmacol.* 94 (2018) 876–884.
- [33] D. Anastasiou, G. Pouligiannis, J.M. Asara, M.B. Boxer, J.K. Jiang, M. Shen, G. Bellinger, A.T. Sasaki, J.W. Locasale, D.S. Auld, et al., Inhibition of pyruvate kinase M2 by reactive oxygen species contributes to cellular antioxidant responses, *Science* 334 (2011) 1278–1283.
- [34] Z. Liu, Y. Le, H. Chen, J. Zhu, D. Lu, Role of PKM2-mediated immunometabolic reprogramming on development of cytokine storm, *Front. Immunol.* 12 (2021) 748573.
- [35] J.B. Ye, J. Fan, S. Venneti, Y.W. Wan, B.R. Pawel, J. Zhang, L.W.S. Finley, C. Lu, T. Lindsten, J.R. Cross, et al., Serine catabolism regulates mitochondrial redox control during hypoxia, *Cancer Discov.* 4 (2014) 1406–1417.
- [36] T. Teslaa, M. Ralser, J. Fan, J.D. Rabinowitz, The pentose phosphate pathway in health and disease, *Nat. Metab.* 5 (2023) 1275–1289.
- [37] N.M. Grüning, M. Rinnerthaler, K. Blumlein, M. Müllleder, M.M.C. Wamelink, H. Lehrach, C. Jakobs, M. Breitenbach, M. Ralser, Pyruvate kinase triggers a metabolic feedback loop that controls redox metabolism in respiring cells, *Cell Metabol.* 14 (2011) 415–427.
- [38] R.H. Gottfredsen, U.G. Larsen, J.J. Enghild, S.V. Petersen, Hydrogen peroxide induce modifications of human extracellular superoxide dismutase that results in enzyme inhibition, *Redox Biol.* 1 (2013) 24–31.
- [39] L. Ramanathan, S. Gulyani, R. Nienhuis, J.M. Siegel, Sleep deprivation decreases superoxide dismutase activity in rat hippocampus and brainstem, *Neuroreport* 13 (2002) 1387–1390.
- [40] R. Nault, K.A. Fader, S. Bhattacharya, T.R. Zacharewski, Single-nuclei RNA sequencing assessment of the hepatic effects of 2,3,7,8-Tetrachlorodibenzo-p-dioxin, *Cell Mol Gastroenter* 11 (2021) 147–159.